Electrochemical development of magnetic long-range correlations with Tc?=?128?K in a tetraoxolene-bridged Fe-based framework

doi: 10.1016/j.jmmm.2019.165818

Electrochemical Development of Magnetic Long-Range Correlations with T_c = 128 K in a Tetraoxolene-Bridged Fe-Based Framework

Jian Chen,[a,b] Kouji Taniguchi,[a,b,c] Yoshihiro Sekine,[a,b] and Hitoshi Miyasaka[a,b,*]

[a] Institute for Materials Research, Tohoku University, 2-1-1 Katahira, Aoba-ku, Sendai 980-8577, Japan

[b] Department of Chemistry, Graduate School of Science, Tohoku University, 6-3 Aramaki-Aza-Aoba, Aoba-ku, Sendai 980-8578, Japan

[c] Elements Strategy Initiative for Catalysts and Batteries (ESICB), Kyoto University, Kyoto 615-8520, Japan

Corresponding author*
Prof. Dr. Hitoshi Miyasaka
Institute for Materials Research
Tohoku University
2–1–1 Katahira, Aoba-ku, Sendai 980-8577, Japan
E-mail: miyasaka@imr.tohoku.ac.jp
Tel: +81-22-215-2030
FAX: +81-22-215-2031

Abstract

The generation of the paramagnetic radical ($Cl_2An^{\bullet 3-}$) in the framework-edge moieties of an Fe-based two-dimensional honeycomb framework with 2,5-dichloro-3,6-dihydroxy-1,4-benzoquinonate (Cl_2An^{n-}), $(H_3O)_2(phz)_3[Fe_2(Cl_2An)_3]$ (phz = phenazine), allowed the formation of long-range magnetic correlations over the network with a relative high magnetic phase transition temperature (T_c) of 128 K. The original compound is a paramagnet with a diamagnetic Cl_2An^{2-} linker that significantly separates paramagnetic Fe^{II} ions ($S = 2$), where the $[(H_3O)_2(phz)_3]^{2+}$ cation is located between layered frameworks. Post-synthetic electron-doping, i.e., reduction in the solid state, using a lithium-ion battery (LIB) system, finally produced $(Li^+)_3(H_3O^+)_2(phz)_3[(Fe^{2+})_2(Cl_2An^{\bullet 3-})_3]$, which demonstrated a drastic magnetic change.

Keywords: Fe-tetraoxolene complex; two-dimensional honeycomb framework; postsynthetic method; electron-doping; lithium ion battery; molecular magnets

■ Introduction

The design of molecular magnets with a high magnetic phase transition temperature (T_c) is a longstanding theme in the field of molecular materials science.[1−5] A class of metal–organic frameworks (MOFs) with paramagnetic metal ions (*M*) bridged by π-conjugated organic linkers (L) is one of the promising candidates for molecular magnets because superexchange magnetic coupling between metal spins is anticipated through π-frontier orbitals.[6−8] However, with nonmagnetic organic linkers, most MOFs only show paramagnetic behavior or weak magnetic correlations resulting from long-distance superexchange interactions through π-orbital overlapping over the linker between metal spins (left in Scheme 1).[9−11] To improve this, the introduction of paramagnetic spin (S = 1/2) into the linker molecule, *i. e.*, the use of organic radical ligands as a linker or post-synthetically generating a radical state in the original linker, could be an effective strategy to enhance the magnetic correlations, which could stabilize the magnetic ordering state with a help of the newly produced kinetic exchange interaction between the radical spin and transition metal center (right in Scheme 1).[12,13]

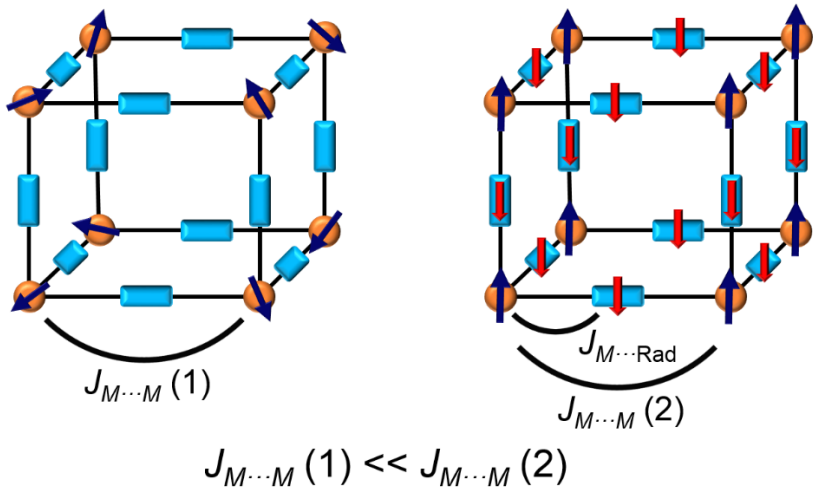

Scheme 1. Magnetic correlation between metal spins through nonmagnetic organic linkers (left) and organic radicals (right). $J_{M\cdots M}$ represents the magnetic interaction (J) between the metal spins, and $J_{M\cdots Rad}$ represents J between the metal and radical spins. Orange spheres and blue blocks represent the metal ions and organic linkers, respectively. The dark blue and red arrows represent the magnetic spins of the metals and radicals.

We have proposed using intra-lattice electron transfer between electron donor (D) and electron acceptor (A) subunits in π-conjugated MOFs to generate the spin set of $D^+(\uparrow) - A^-(\downarrow)$ coupled by

a finite-sized exchange interaction as well as coulombic charge-separation. If D or A is a π-conjugated organic redox species, the generated spin is a radical spin that possibly enables the formation of dπ–pπ conjugation with metal centers. For example, assembly reactions of a family of carboxylate-bridged paddlewheel-type diruthenium(II, II) complexes ($[Ru_2^{II,II}]$) that act as a D-subunit and organic electron-acceptors (*i.e.*, A-subunits) of TCNQ and DCNQI derivatives (TCNQ = 7,7,8,8-tetracyano-*p*-quinodimethane; DCNQI = *N,N′*-dicyanoquinonediimine) allow the construction of multi-dimensional coordination polymers with the formula of DA for one-dimensional chains or D_2A for ladder chains, two-dimensional layers, and three-dimensional infinite networks.[14] Importantly, the magnetic properties of these DA or D_2A assemblies are strongly dependent on whether intra-lattice electron-transfers occur during the course of the assembly process: the D^+A^- species are ferrimagnetic chains,[15] and when the $D^{0.5+}{}_2A^-$ layers or infinite networks are spontaneous magnets of either ferrimagnets[16] or antiferromagnets,[17] whereas D^0A^0 and $D^0{}_2A^0$ are paramagnetic, as well as $D^+{}_2A^{2-}$.[18] In the $D^{0.5+}{}_2A^-$ system, the radical spin on the TCNQ moiety mediates an exchange interaction between $[Ru_2]^{0/+}$ spins, which demonstrates ferrimagnetic spin ordering over the framework; e.g., the three-dimensional network compound at T_c = 107 K.[19] Another example was found in a family of coordination polymers with 2,5-dichloro-3,6-dihydroxy-1,4-benzoquinonate (Cl_2An^{n-}), in which Cl_2An^{n-} acts as a redox-active species with three different charge states of n = 2, 3, or 4 (Scheme 2).[13, 20] A two-dimensional D_2A_3 honeycomb system, $(Me_2NH_2)_2[Fe_2(Cl_2An)_3]\cdot 2H_2O\cdot 6DMF$, where the Fe^{II} ion is D,[13] exhibited ferrimagnetic ordering via radical spin in $Cl_2An^{\bullet 3-}$ that was formed by electron-transfer from each Fe^{II} ion to Cl_2An^{2-}.

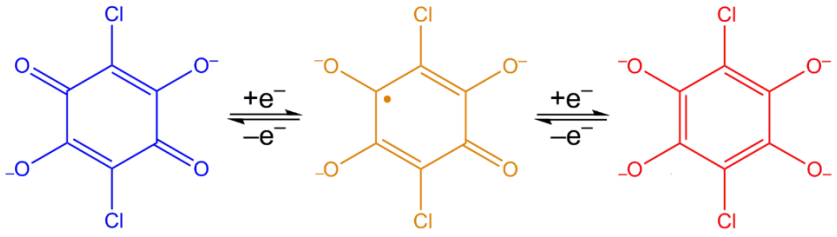

Scheme 2. Changes in the oxidation state of Cl_2An^{n-}: left to right, n = 2, 3, 4.

The post-synthetic generation of radical species in a framework is also efficient for the design of magnetic MOFs. One radical-generation technique is to use solid-state bulk electrochemistry, in which stimulus redox activation of the subunits in a target MOF should be achieved at the electrode,

which concurrently involves counter ion insertion/extraction that neutralizes the material. This technique was demonstrated in a lithium-ion battery (LIB) system, in which electrochemical reduction of the neutral acceptor subunits in the redox-active MOF at the cathode (i.e., discharge process for the cathode material) produced a radical spin state between paramagnetic metal centers as well as Li^+ insertion (Fig. 1a). Consequently, the electron-reduced MOF, $(Li^+)_x[MOF]^{x-}$, demonstrated the construction of artificial long-range magnetic ordering (Fig. 1b).[21 – 26] A paramagnetic $[Ru_2^{II,II}]$–TCNQ system that has a neutral TCNQ was changed to a high T_c magnet with T_c = 88 K by electrochemical electron doping into a neutral TCNQ moiety via the discharge process of the LIB system.[21,23] Even in the metal–Cl_2An^{n-} honeycomb system mentioned above, the T_c modulation by the LIB system was also demonstrated; a T_c change from 10 K (charged phase) to 36 K (discharged phase) was found in $(NBu_4)[Mn^{II}Cr^{III}(Cl_2An)_3]$.[24] However, the combination of Fe and $Cl_2An^{\bullet 3-}$ is a promising candidate for high-T_c magnets because of the presence of strong exchange coupling between Fe^{III} and $Cl_2An^{\bullet 3-}$.[20,27] In fact, a few relevant compounds of $[Fe_2(Cl_2An)_3]^{n-}$ MOFs (D_2A_3-type) have revealed high T_c magnets; T_c = 80 K for $(Me_2NH_2)_2[Fe_2(Cl_2An)_3]\cdot 2H_2O\cdot 6DMF$[13] and T_c = 105 K for $(Cp_2Co)_{1.43}(Me_2NH_2)_{1.57}[Fe_2(Cl_2An)_3]\cdot 4.9DMF$.[28]

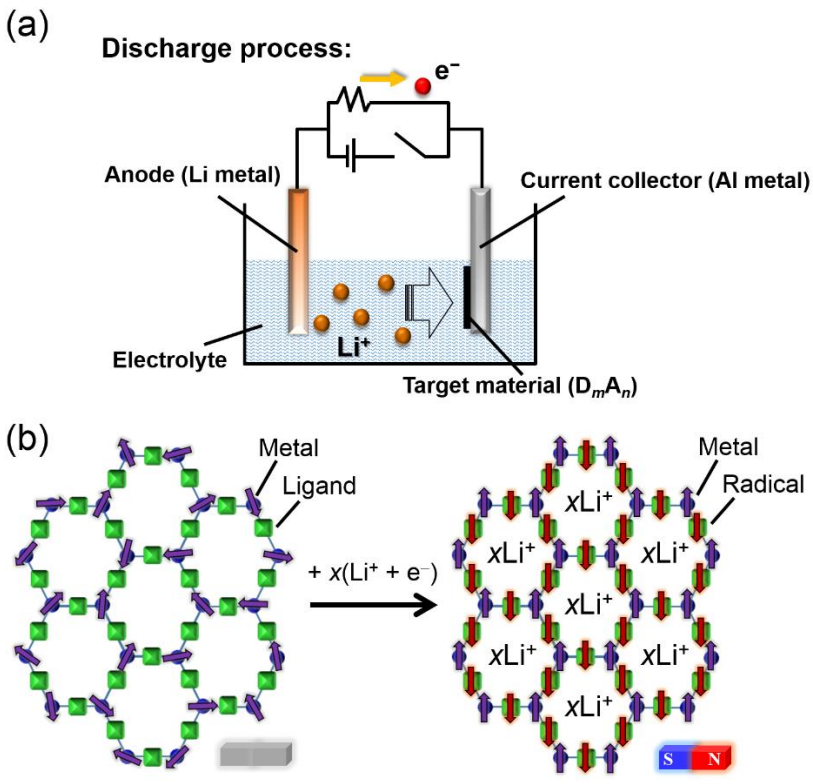

Fig. 1. (a) Schematic illustration of the discharge process in an LIB system. The LIB system consists

of three main parts, anode, electrolyte and cathode, containing the target material (D_mA_n). (b) Schematic representation of the spin state changes in the discharge process from MOF to the electron-reduced MOF, $(Li^+)_x[MOF]^{x-}$. The purple and red arrows represent the magnetic spins of the metals and radicals, respectively.

In this study, we demonstrate electrochemical synthesis of a spontaneous magnet using the paramagnetic Fe–Cl_2An^{2-} honeycomb system, $(H_3O)_2(phz)_3[Fe_2(Cl_2An)_3]$ (**1**), as the precursor.[29] The electron-doped material exhibited long-range ferrimagnetic ordering with T_c = 128 K, which was developed by radical spin generation in the Cl_2An^{2-} moiety in the cathode of **1** through an LIB discharge process.

■ Experimental section

Synthesis of $(H_3O)_2(phz)_3[Fe_2(Cl_2An)_3]$ (1). A solvated form of **1**, which includes acetone and water molecules, $(H_3O)_2(phz)_3[Fe_2(Cl_2An)_3]\cdot(CH_3COCH_3)_n\cdot(H_2O)_n$ (**1-solv**), was prepared by the following method that was previously reported.[29] Compound **1** was then obtained in a 64 % yield by heating at 100 °C under vacuum for 2 days. Elemental analysis calculated for $C_{54}H_{30}Cl_6Fe_2N_6O_{14}$: C 49.46, H 2.31, N 6.41; Found C 49.16, H 2.44, N 6.15. IR (ν_{max}/cm^{-1}, KBr pellets): 3408(m), 3075(w), 1630(m), 1485(vs), 1433(w), 1357(vs), 1263(vw), 1149(w), 1121(m), 1006(m), 856(s), 826(m), 750(s), 610(w), 591(s), 577(s), 506(s), 418(m).

Physical characteristics measurements. Infrared (IR) spectra were recorded using KBr pellets at room temperature with a JASCO FT/IR-4200 spectrometer. Powder X-ray diffraction (PXRD) patterns were measured for **1** using a RIGAKU Ultima IV diffractometer with Cu Kα radiation (λ = 1.5418 Å) at room temperature in a glass capillary (ϕ = 0.5 mm). The PXRD measurements were conducted at a rate of 0.1 º min^{-1} with a step length of 0.02 º. Structural characterization of **Cath-init** and **Cath-red** (*vide infra*) was performed by *ex situ* PXRD using a RIGAKU Ultima IV diffractometer with Cu Kα radiation (λ = 1.5418 Å) at a rate of 1 º min^{-1} with a step length of 0.02 º at room temperature. Thermogravimetric analyses (TGA) were recorded on a Shimadzu DTG-60H apparatus under a flowing N_2 atmosphere from 20 to 500 ºC at a heating rate of 5 ºC min^{-1}. X-band electron spin resonance (ESR) spectra were recorded on a JEOL spectrometer at 9.08 GHz for cathode samples of the LIB at room temperature. Magnetic properties were measured with a SQUID magnetometer (MPMS-XL, Quantum Design, U.S.A.). Magnetization measurements were performed by applying a

DC magnetic field in the temperature range of 1.8 to 300 K. Field dependence of the magnetization measurements were performed between −5 and +5 T at 5 K. The crystal structures were prepared using VESTA software.[30]

Lithium-ion battery (LIB) cell preparation. The lithium ions and electrons were introduced to the target compound using an LIB system to improve the ordering temperature, T_c, via radical spin generation. The cathode of LIB was prepared by mixing the ground target material, **1**, acetylene black (as a conductive medium) and polytetrafluoroethylene (PTFE; as a binder) in a mass ratio of 5;4;1, respectively. Then, the cathode material was pressed on the current collector of the aluminum net and dried overnight at 60 ºC under vacuum. An $LiPF_6$ electrolyte was dissolved at 1 mol/dm^3 in ethylene carbonate: dimethyl carbonate that had a 3:7 volume ratio, respectively. The coin-type cell (2032-type) was assembled with the cathode, anode, separator and electrolyte in an Ar-filled glovebox.

Lithium-ion insertion process. A galvanostatic intermittent titration technique (GITT) was employed to insert lithium ions into **1**.[31] During the insertion process, LIB was under a discharge process for 1 h at a constant low-density current (5.11 mA/g), and then in an open circuit state for 1 h to allow the entire system to reach an electrochemical equilibrium state. The open circuit voltage (OCV) was recorded with a potentiogalvanostat (Solartron, 1470E) at 25 ºC. After the discharge process, the coin cells were disassembled, and the **1** cathodes were extracted in the Ar-filled glovebox.

■ Results and discussion

To achieve post-synthetic electron-doping using an LIB system, one necessity is that the target compound should be a porous material, i.e., a MOFs, to accommodate the Li^+ ions introduced by the discharge process. Thus, the first trial was to identify the stable, porous, and solvent-free material that is produced by removing the crystallization solvents from the solvated material. The solvated form of **1**, $(H_3O)_2(phz)_3[Fe_2(Cl_2An)_3]\cdot(CH_3COCH_3)_n\cdot(H_2O)_n$ (**1-solv**), which includes acetone and water molecules, has already been previously reported.[29] The TGA diagram of the freshly prepared, solvated sample, **1-solv**, shows a gradual weight loss of up to ~200 ºC and significant weight loss above that temperature, corresponding to removal of guest acetone and water molecules (Fig. S1). In fact, **1**, which was obtained by removing the crystal solvent from **1-solv**, exhibited little weight loss within 150 ºC (Fig. S1). The formula for **1** is in good agreement with the desolvated composition derived from **1-solv**: $C_{54}H_{30}Cl_6Fe_2N_6O_{14}$ (see Experimental Section). It was difficult to obtain

compound **1** in high enough quality for single-crystal X-ray structural analysis; however, comparison of the PXRD patterns of **1** and $(H_3O)_2(phz)_3[Cu_2(Cl_2An)_3]$, the structure of which was known,[32] revealed that **1** is isostructural with $(H_3O)_2(phz)_3[Cu_2(Cl_2An)_3]$ and has a Cl_2An-bridged Fe–based two-dimensional honeycomb framework with counter cations of $[(H_3O)_2(phz)_3]^{2+}$ located between the layers (Fig. S2). The packing structure is composed of alternating anionic layers $[M_2(Cl_2An)_3]^{2-}$ (M = Cu, Fe) and cationic layers $[(H_3O)_2(phz)_3]^{2+}$ via π-π stacking, forming a nanoscale hexagonal 1D channel along the c axis (Fig. 2). The anionic layer of $[M_2(Cl_2An)_3]^{2-}$ consists of metal ions coordinated with six O atoms originating from three different Cl_2An^{2-} bridging ligands. Meanwhile, the cationic layer of $[(H_3O)_2(phz)_3]^{2+}$ has a supramolecular cationic form that consists of hydroxonium ions and phenazine connected via hydrogen bonds.[32] Note that **1** was freshly prepared in this work.

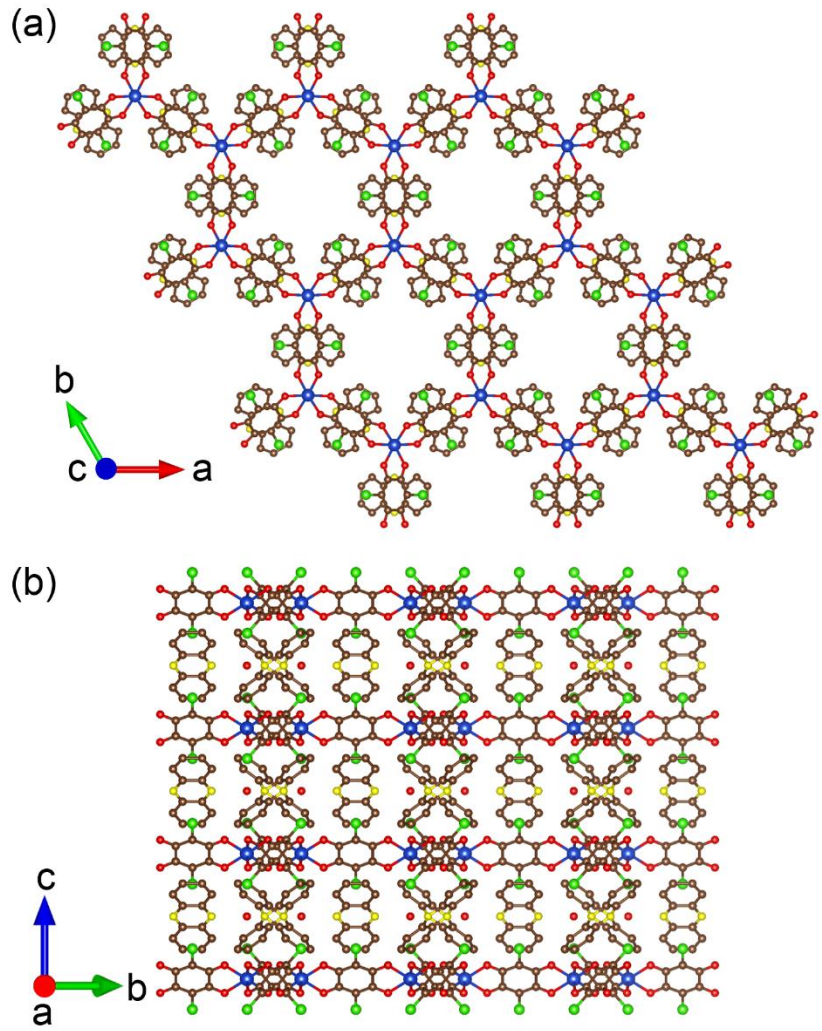

Fig. 2. Packing structure of alternating anionic layers of $\{[M_2(Cl_2An)_3]^{2-}\}_n$ and cationic layers of $\{[(H_3O)_2(phz)_3]^{2+}\}_n$: (a) Viewed along the crystallographic c axis; (b) Viewed along the

crystallographic *a* axis. Blue, brown, red, green, and yellow spheres represent *M*, C, O, Cl, and N atoms, respectively. Hydrogen atoms are omitted for clarity.

The temperature (*T*) dependence of the field-cooled magnetization (FCM; M_m) of **1** was measured under a 1 kOe magnetic field in the temperature range of 300 to 1.8 K; Fig. 3 depicts a plot of the magnetic susceptibility ($\chi_m = M_m/H$). The $\chi_m T$ product at 300 K was 8.4 cm^3 K mol^{-1}. The $\chi_m T$ product gradually increased upon cooling the temperature to a maximum of 15.8 cm^3 K mol^{-1} at 7.4 K, followed by an abrupt decrease to 8.7 cm^3 K mol^{-1} at 2.0 K. The spins in **1** basically originated from Fe^{II} centers, which could be realized because the signal of electron spin resonance (ESR) was barely visible for **1** (red curve in Fig. 4) (*vide infra*). The increase in $\chi_m T$ indicates that ferromagnetic interactions are dominant between Fe^{II} ions in the layered network of **1**. However, the magnetic field dependence of the magnetization (*M*–*H*) at 5 K showed no hysteresis, indicating the absence of magnetic long-range ordering even at 5 K (inset of Fig. 3). This magnetic behavior in **1** is very similar to the behavior of **1-solv** that was already reported: short-range ferromagnetic correlations were constructed among Fe^{II} ions via neutral Cl_2An^{2-} in the network. This magnetic feature implies that **1** is suitable as a cathode material of an LIB because it can form long-range magnetic ordering by generating the radical ligand ($Cl_2An^{\bullet 3-}$) from Cl_2An^{2-} via a discharge process (Fig. 1).

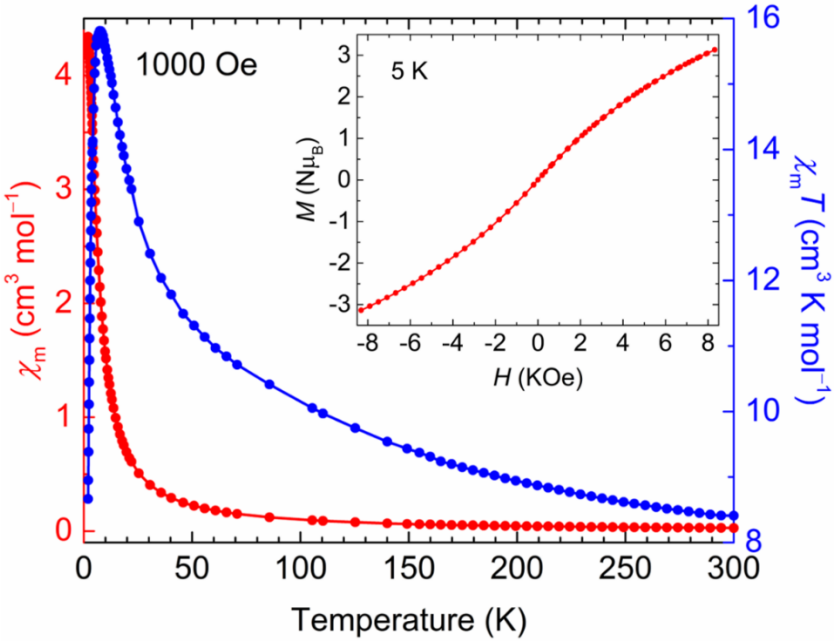

Fig. 3. Temperature dependence of χ_m (red line) and $\chi_m T$ (blue line) measured at H_{dc} = 1 kOe ($\chi_m = M_m/H_{dc}$) for **1**. Inset: magnetic field dependence of magnetization measured at 5 K in the low field region.

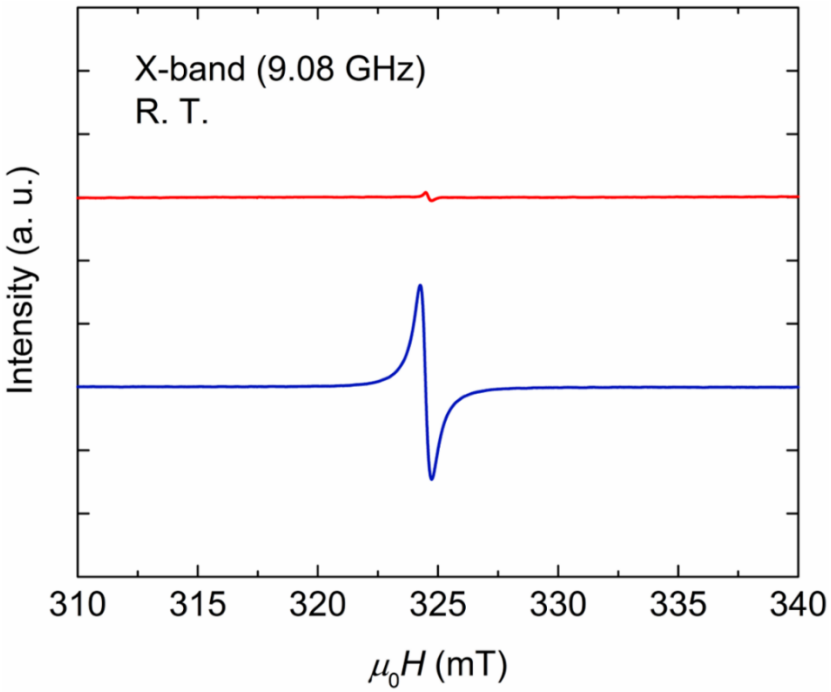

Fig. 4. ESR spectra of Cath-init (top, red line) and Cath-red (bottom, blue line) at room temperature.

An LIB system with a cathode incorporating **1** was constructed (Fig. S3). Figure 5a shows the open circuit voltage (OCV) for the discharge process as a function of capacity, which is the electric charge quantity per unit weight. During the discharge process, electrons and Li^+ were simultaneously introduced into the cathode, leading to an increase in chemical potential for electrons in the cathode material. Thus, a decrease in the OCV (*vs.* Li/Li+) during the discharge process corresponds to the variation of the difference in equilibrium electrochemical potentials for electrons between the cathode and anode in the used electrolyte.[33] The absolute value of the derivative of capacity (Q) with respect to voltage (V), $|dQ/dV|$, gave a distinct peak at approximately 2.82 V *vs*. Li/Li^+ (Fig. 5b), which corresponds to a reduction potential of **1**. Only one reduction peak was observed during the discharge process in the OCV range of 3.16–2.67 V *vs.* Li/Li^+. Considering that the respective reduction potential of Fe^{II} is reported around ~1.0 V *vs* Li/Li^+,[34–37] which is much lower than the electric potential observed during the discharge process (2.6~3.2 V *vs.* Li/Li^+), the possibility of reduction in the Fe^{II} centers can be excluded. In addition, the redox potential of $Cl_2An^{2-}/Cl_2An^{\bullet 3-}$ is reported around the observed potential (~2.6 V *vs.* Li/Li^+).[24,38] So the reduction potential observed at 2.82 V *vs*. Li/Li^+, should correspond to the ligand-based reduction of $Cl_2An^{2-} + e^- \rightarrow Cl_2An^{\bullet 3-}$. The initial cathode sample taken at 3.16 V *vs*. Li/Li^+ ($x = 0$) and the significantly reduced cathode sample taken at 2.67 V *vs*. Li/Li^+ ($x = 3$) are hereafter called as **Cath-init** and **Cath-red**, respectively, where x is the nominal Li composition per formula unit estimated from the discharged capacity. The structural stability of the discharge process was checked using *ex situ* PXRD measurements for **Cath-red** (Fig.

S4). The peaks indicating the basic layered structure of **1** was maintained for **Cath-red**, although they were weakened and some additional peaks emerged. The shift of some peaks and the change of relative intensity in PXRD pattern might be caused by the different complex stacking mode of the anionic layers ($[Fe_2(Cl_2An)_3]^{2-}$), which is induced by the insertion of new kind of cations (Li^+) after discharge process, from the original stacking mode.

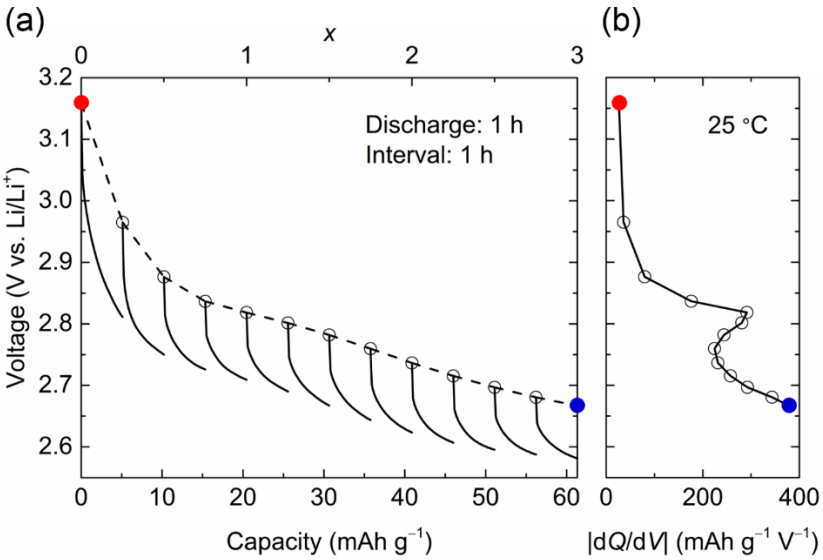

Fig. 5. Open circuit voltage (OCV) curves. (a) OCV as a function of capacity for an LIB coin cell combined with **1**. The solid lines represent the voltage change during the discharge process at a constant current. The dashed line represent the variation tendency of each electrochemical equilibrium state (open circles). The red and blue closed circles display the **Cath-init** and **Cath-red** *ex situ* physical measurements, respectively. The upper abscissa indicates the nominal Li composition (x) per formula unit estimated from the discharged capacity. (b) Absolute values of the derivative of the capacity (Q) with respect to the voltage (V), $|dQ/dV|$.

To investigate the details of the charge state change during the discharge process, we conducted *ex situ* electron spin resonance (ESR) measurements for **Cath-red** and **Cath-init**. The OCVs of the measured samples are displayed by the corresponding colored spots (red for **Cath-init** with $x = 0$ and blue for **Cath-red** with $x = 3$) in Fig. 5. The spectrum of **Cath-red** exhibited a sharp ESR signal at a magnetic field of $g \sim 2$ (Fig. 4), whereas the spectrum of **Cath-init** had a very weak signal at $g \sim 2$ (impurity; *vide infra*). Considering that the charge of Fe is basically +2 in **1** and **Cath-init**, the observed sharp signal for **Cath-red** should be attributed to the $Cl_2An^{\bullet 3-}$ radical generated by the reduction of the Cl_2An^{2-} moiety. The small signal observed for **Cat-init** is probably due to an impurity originating from structural defects that include $Cl_2An^{\bullet 3-}$ and/or Fe^{3+} spontaneously generated during the formation of **1** from **1-solv**.

Figure 6 displays the temperature dependence of FCM at H = 100 Oe and the remnant magnetization (RM) for **Cath-init** and **Cath-red**. As confirmed from the vanishing temperature of RM, long-range ferrimagnetic ordering occurred at 128 K (= T_c) for **Cath-red**. This resulted from the formation of magnetic correlations between Fe^{II} ions with S = 2 through the radical spin of $Cl_2An^{\bullet 3-}$ that was post-synthetically formed by electrochemistry. The superexchange magnetic coupling between Fe^{II} ions with S = 2 and $Cl_2An^{\bullet 3-}$ with S = 1/2 is expected to be antiferromagnetic; thus, the spontaneous magnetic ordering could be due to a ferrimagnetic state. In the previous work on magnetic change in LIB, $(NBu_4)[Mn^{II}Cr^{III}(Cl_2An)_3]$ provided a T_c of 36 K during the discharge process.[24] These results confirm that the combination of transition metal ions with the $Cl_2An^{\bullet 3-}$ radical, namely mutual energy levels of SOMOs (SOMO = singly occupied molecular orbital), are quite important to tune the magnetic superexchange interactions and T_c. Of note, the combination of the $Cl_2An^{\bullet 3-}$ radical and Fe^{III} ions also revealed a relative high T_c.[13,28]

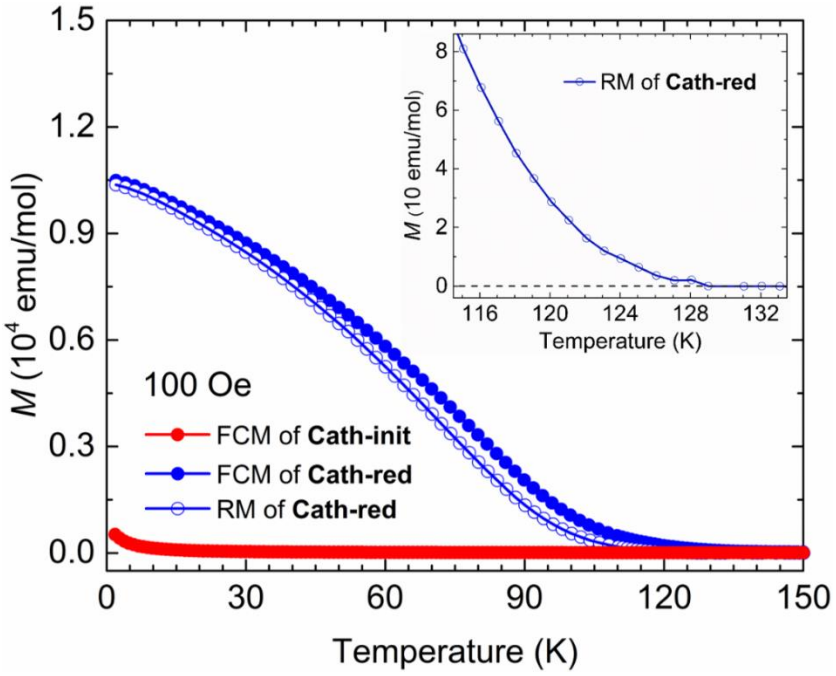

Fig. 6. Temperature dependence of the field-cooled magnetization (FCM) measured at H_{dc} = 100 Oe and the remnant magnetization (RM) of the cathode material. The red closed circles represent the FCM of **Cath-init**. The blue closed and open circles represent FCM and RM of **Cath-red**, respectively. Inset: enlarged drawing of RM of **Cath-red** between 114 K and 134 K.

The magnetic field dependence of the magnetization for **Cath-red** was measured at 5 K (Fig. 7). The magnetization (M_m/N) value measured at H = 5 T for **Cath-red** was 5.1 μ_B, which was smaller

than 6.1 μ_B (H = 5 T) for **Cath-init** with two paramagnetic S = 2 spins on the Fe^{2+} species. This could be ascribed to the antiferromagnetic spin arrangement of S = 2 on Fe^{2+} ions and S = 1/2 on $Cl_2An^{\bullet 3-}$ formed during the discharge process. The presumable saturated M value for $(Li^+)_3\{(H_3O^+)_2(phz)_3[(Fe^{2+})_2(Cl_2An^{\bullet 3-})_3]\}$ with x = 3 should be approximately 5.8 μ_B, assuming Fe^{2+} (S = 2, g = 2.2)[27] and $Cl_2An^{\bullet 3-}$ (S = 1/2, g = 2.0)[20].

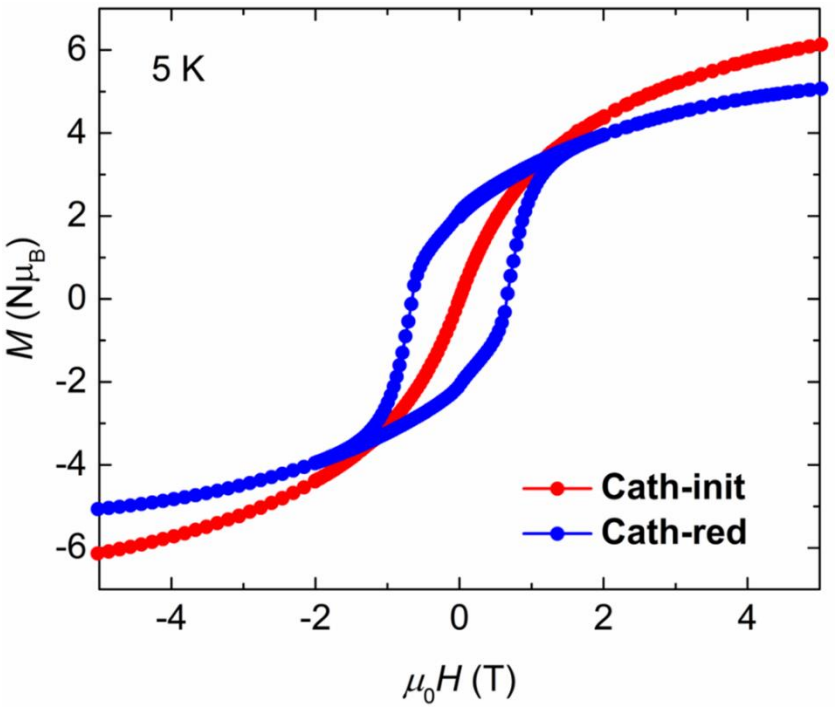

Fig. 7. Magnetic field dependence of the magnetization (M–H) of **Cath-init** (red) and **Cath-red** (blue) at 5 K.

■ Conclusion

In this study, we succeeded in electrochemically developing long-range ferrimagnetic correlations based on an LIB system in the paramagnetic MOF, $(H_3O)_2(phz)_3[Fe_2(Cl_2An)_3]$ (**1**), which has a honeycomb layer comprising Fe^{II} ions and Cl_2An^{2-} as nodes and edges, respectively. The cathode material that included **1** was electrochemically reduced and involved insertion of Li^+ ions during the discharge process, wherein the Cl_2An^{2-} moiety was electron-doped following the reaction $Cl_2An^{2-} + e^- \rightarrow Cl_2An^{\bullet 3-}$. This created antiferromagnetic superexchange interactions between the Fe^{II} ions and the $Cl_2An^{\bullet 3-}$ radical edges. The fully electron-doped compound, $(Li^+)_3(H_3O^+)_2(phz)_3[Fe^{2+}{}_2(Cl_2An^{\bullet 3-})_3]$, was presumably in the electron-doped cathode material, which finally showed a high T_c of 128 K.

■ Acknowledgements

We thank Prof. T. Akutagawa and Dr. N. Hoshino (Tohoku University) for their help with the ESR measurements. This work was supported by Grants-in-Aid for Scientific Research (Grant Nos. 16K05738 and 16H02269), Grants-in-Aid for Scientific Research in Innovative Areas (Grant no. JP17H05137; 'π-System Figuration' Area 2601, Grant no. JP17H05350; 'Coordination Asymmetry' Area 2802) from JSPS, the MEXT program 'Elements Strategy Initiative to Form a Core Research Center' (since 2012) from the Ministry of Education, Culture, Sports, Science, and Technology, Japan, a Support Program for Interdisciplinary Research (FRIS project), the E-IMR project, the Kato Foundation for Promotion of Science, the Iketani Science and Technology Foundation, and the Shorai Foundation for Science and Technology. J. C. gratefully acknowledges financial support from the Chinese Scholarship Council (CSC) and Institute for Materials Research, Tohoku University.

References

[1] V. Gadet, T. Mallah, I. Castro, M. Verdaguer, High-T_c Molecular-Based Magnets: A Ferromagnetic Bimetallic Chromium(III)-Nickel(II) Cyanide with T_c = 90 K, J. Am. Chem. Soc. 114 (1992) 9213−9214.

[2] W. R. Entley, G. S. Girolami, High-Temperature Molecular Magnets Based on Cyanovanadate Building Blocks: Spontaneous Magnetization at 230 K, Science 268 (1995) 397−400.

[3] J. M. Manriquez, G. T. Yee, R. S. Mclean, A. J. Epstein, J. S. Miller, A Room-Temperature Molecular/Organic-Based Magnet, Science 252 (1991) 1415−1417.

[4] J. S. Miller, Magnetically Ordered Molecule-Based Materials, Chem. Soc. Rev. 40 (2011) 3266−3296.

[5] E. Coronado, G. M. Espallargas, Dynamic Magnetic MOFs, Chem. Soc. Rev. 42 (2013) 1525−1539.

[6] H. Tamaki, Z. J. Zhong, N. Matsumoto, S. Kida, M. Koikawa, N. Achiwa, Y. Hashimoto, H. Ōkawa, Design of Metal-Complex Magnets. Syntheses and Magnetic Properties of Mixed-Metal Assemblies $\{NBu_4[MCr(ox)_3]\}_x$ (NBu_4^+ = Tetra(*n*-butyl)ammonium Ion; ox^{2-} = Oxalate Ion; M = Mn^{2+}, Fe^{2+}, Co^{2+}, Ni^{2+}, Cu^{2+}, Zn^{2+}), J. Am. Chem. Soc. 114 (1992) 6974−6979.

[7] E. Coronado, J. R. Galán-Mascarós, C. J. Gómez-García, V. Laukhin, Coexistence of Ferromagnetism and Metallic Conductivity in a Molecule-Based Layered Compound, Nature 408 (2000) 447−449.

[8] M. Kurmoo, Magnetic Metal–Organic Frameworks, Chem. Soc. Rev. 38 (2009) 1353−1379.

[9] S. Benmansour, C. Vallés-García, P. Gómez-Claramunt, G. M. Espallargas, C. J. Gómez-García, 2D and 3D Anilato-Based Heterometallic M(I)M(III) Lattices: The Missing Link, Inorg. Chem. 54 (2015) 5410−5418.

[10] S. R. Batten, P. Jensen, C. J. Kepert, M. Kurmoo, B. Moubaraki, K. S. Murray, D. J. Price, Syntheses, Structures and Magnetism of α-$Mn(dca)_2$, $[Mn(dca)_2(H_2O)_2]\cdot H_2O$, $[Mn(dca)_2(C_2H_5OH)_2]\cdot(CH_3)_2CO$, $[Fe(dca)_2(CH_3OH)_2]$ and $[Mn(dca)_2(L)_2]$, where L = pyridine, CH_3OH or DMF and dca^- = dicyanamide, $N(CN)_2^-$, J. Chem. Soc., Dalton Trans. (1999) 2987−2997.

[11] M. Atzori, S. Benmansour, G. M. Espallargas, M. Clemente-León, A. Abhervé, P. Gómez-Claramunt, E. Coronado, F. Artizzu, E. Sessini, P. Deplano, A. Serpe, M. L. Mercuri, C. J. G. García, A Family of Layered Chiral Porous Magnets Exhibiting Tunable Ordering Temperatures, Inorg. Chem. 52 (2013) 10031−10040.

[12] K. S. Pedersen, P. Perlepe, M. L. Aubrey, D. N. Woodruff, S. E. Reyes-Lillo, A. Reinholdt, L. Voigt, Z. S. Li, K. Borup, M. Rouzières, D. Samohvalov, F. Wilhelm, A. Rogalev, J. B. Neaton, J. R. Long, R. Clérac, Formation of the Layered Conductive Magnet $CrCl_2(pyrazine)_2$ through Redox-Active Coordination Chemistry, Nat. Chem. 10 (2018) 1056−1061.

[13] I. R. Jeon, B. Negru, R. P. Van Duyne, T. D. Harris, A 2D Semiquinone Radical-Containing Microporous Magnet with Solvent-Induced Switching from T_c = 26 to 80 K, J. Am. Chem. Soc. 137 (2015) 15699−15702.

[14] H. Miyasaka, Control of Charge Transfer in Donor/Acceptor Metal-Organic Frameworks, Accounts Chem. Res. 46 (2013) 248−257.

[15] Y. Sekine, T. Shimada, H. Miyasaka, Ionic Donor-Acceptor Chain Derived from an Electron-Transfer Reaction of a Paddlewheel-Type Diruthenium(II, II) Complex and *N,N'*-Dicyanoquinonediimine, Chem. Eur. J. 24 (2018) 13093−13097.

[16] W. Kosaka, H. Fukunaga, H. Miyasaka, Electron-Transferred Donor/Acceptor Ferrimagnet with T_C = 91 K in a Layered Assembly of Paddlewheel $[Ru_2]$ Units and TCNQ, Inorg. Chem. 54 (2015), 10001−10006.

[17] H. Miyasaka, N. Motokawa, S. Matsunaga, M. Yamashita, K. Sugimoto, T. Mori, N. Toyota, K. R. Dunbar, Control of Charge Transfer in a Series of $Ru_2^{II,II}$/TCNQ Two-Dimensional Networks by Tuning the Electron Affinity of TCNQ Units: A Route to Synergistic Magnetic/Conducting Materials, J. Am. Chem. Soc. 132 (2010), 1532−1544.

[18] W. Kosaka, T. Morita, T. Yokoyama, J. Zhang, H. Miyasaka, Fully Electron-Transferred Donor/Acceptor

Layered Frameworks with $TCNQ^{2-}$, Inorg. Chem. 54 (2015) 1518−1527.

[19] N. Motokawa, H. Miyasaka, M. Yamashita, K. R. Dunbar, An Electron-Transfer Ferromagnet with T_c = 107 K Based on a Three-Dimensional $[Ru_2]_2$/TCNQ System, Angew. Chem. Int. Ed. 47 (2008) 7760−7763.

[20] J. Chen, Y. Sekine, Y. Komatsumaru, S. Hayami, H. Miyasaka, Thermally Induced Valence Tautomeric Transition in a Two-Dimensional Fe-Tetraoxolene Honeycomb Network, Angew. Chem. Int. Ed. 57 (2018) 12043−12047.

[21] K. Taniguchi, K. Narushima, J. Mahin, W. Kosaka, H. Miyasaka, Construction of an Artificial Ferrimagnetic Lattice by Lithium Ion Insertion into a Neutral Donor/Acceptor Metal-Organic Framework, Angew. Chem. Int. Ed. 55 (2016) 5238−5242.

[22] K. Taniguchi, K. Narushima, H. Sagayama, W. Kosaka, N. Shito, H. Miyasaka, In Situ Reversible Ionic Control for Nonvolatile Magnetic Phases in a Donor/Acceptor Metal-Organic Framework, Adv. Funct. Mater. 27 (2017) 1604990.

[23] K. Taniguchi, K. Narushima, K. Yamagishi, N. Shito, W. Kosaka, H. Miyasaka, Magneto-Ionic Phase Control in a Quasi-Layered Donor/Acceptor Metal-Organic Framework by Means of a Li-ion Battery System, Jpn. J. Appl. Phys. 56 (2017), 060307.

[24] K. Taniguchi, J. Chen, Y. Sekine, H. Miyasaka, Magnetic Phase Switching in a Tetraoxolene-Bridged Honeycomb Ferrimagnet Using a Lithium Ion Battery System, Chem. Mater. 29 (2017) 10053−10059.

[25] H. Fukunaga, M. Tonouchi, K. Taniguchi, W. Kosaka, S. Kimura, H. Miyasaka, Magnetic Switching by the In Situ Electrochemical Control of Quasi-Spin-Peierls Singlet States in a Three-Dimensional Spin Lattice Incorporating TTF-TCNQ Salts, Chem. Eur. J. 24 (2018) 4294−4303.

[26] K. Taniguchi, N. Shito, H. Fukunaga, H. Miyasaka, Charge-Transfer Layered Assembly of a Trans-Heteroleptic Paddlewheel-Type Diruthenium(II, II) Complex with a TCNQ Derivative: Electrochemical Tuning of the Magnetism, Chem. Lett. 47 (2018) 664−667.

[27] J. A. DeGayner, K. Y. Wang, T. D. Harris, A Ferric Semiquinoid Single-Chain Magnet via Thermally-Switchable Metal−Ligand Electron Transfer, J. Am. Chem. Soc. 140 (2018) 6550−6553.

[28] J. A. DeGayner, I. R. Jeon, L. Sun, M. Dincă, T. D. Harris, 2D Conductive Iron-Quinoid Magnets Ordering up to T_c = 105 K via Heterogenous Redox Chemistry, J. Am. Chem. Soc. 139 (2017), 4175−4184.

[29] G. V. Shilov, Z. K. Nikitina, N. S. Ovanesyan, S. M. Aldoshin, V. D. Makhaev, Phenazineoxonium Chloranilatomanganate and Chloranilatoferrate: Synthesis, Structure, Magnetic Properties, and Mössbauer Spectra, Russ. Chem. Bull. 60 (2011) 1209−1219.

[30] K. Momma, F. Izumi, VESTA 3 for Three-Dimensional Visualization of Crystal, Volumetric and Morphology Data, J. Appl. Cryst. 44 (2011) 1272−1276.

[31] W. Weppner, R. A. Huggins, Determination of the Kinetic Parameters of Mixed-Conducting Electrodes and Application to the System Li_3Sb, J. Electrochem. Soc. 124 (1977) 1569−1578.

[32] T. T. Luo, Y. H. Liu, H. L. Tsai, C. C. Su, C. H. Ueng, K. L. Lu, A Novel Hybrid Supramolecular Network Assembled from Perfect π-π Stacking of an Anionic Inorganic Layer and a Cationic Hydronium-Ion Mediated Organic Layer, Eur. J. Inorg. Chem. (2004) 4253−4258.

[33] J. B. Goodenough, K. S. Park, The Li-Ion Rechargeable Battery: A Perspective, J. Am. Chem. Soc. 135 (2013) 1167−1176.

[34] P. Poizot, S. Laruelle, S. Grugeon, L. Dupont, J. M. Tarascon, Nano-Sized Transition-Metaloxides as Negative-Electrode Materials for Lithium-Ion Batteries, Nature 407 (2000) 496−499.

[35] T. G. Kim, J. G. Lee, D. Son, S. Jin, M. G. Kim, B. Park, Reaction Mechanisms of Tridymite Iron Phosphate with Lithium Ions in the Low-Voltage Range, Electrochim. Acta 53 (2007) 1843−1849.

[36] M. X. Gao, P. Zhou, P. Wang, J. H. Wang, C. Liang, J. L. Zhang, Y. F. Liu, FeO/C Anode Materials of High Capacity and Cycle Stability for Lithium-Ion Batteries Synthesized by Carbothermal Reduction, J. Alloy. Comp. 565 (2013) 97−103.

[37] G. Q. Diao, M. S. Balogun, S. Y. Tong, X. Z. Guo, X. Huang, Y. C. Mao, Y. X. Tong, J. Mater. Chem. A

6 (2018) 15274−15283.
[38] Z. P. Song, Y. M. Qian, X. Z. Liu, T. Zhang, Y. B. Zhu, H. J. Yu, M. Otani, H. S. Zhou, A Quinone-Based Oligomeric Lithium Salt for Superior Li-Organic Batteries, Energy Environ. Sci. 7 (2014) 4077−4086.